Simulation of the Evolution of Floor Covering Ceramic Tiles during the Firing.

Guillermo Peris-Fajarnés
Centro de Investigación en Tecnologías Gráficas, Universidad Politécnica de Valencia
Beatriz Defez
Centro de Investigación en Tecnologías Gráficas, Universidad Politécnica de Valencia
Ricardo Serrano
CAD CAM CAE Laboratory, Universidad EAFIT
Oscar E. Ruiz.
CAD CAM CAE Laboratory, Universidad EAFIT

Abstract

In the context of the firing of ceramic tiles the problem of simulating the final shape of the body is relevant because several defects can occur and the tile can be rejected if the conditions of the firing are inadequate for the geometry and materials of the tile. The existing literature on this problem indicates that previous works present limitations in aspects such as not using a model characteristic of ceramics at high temperatures and oversimplifying the problem. As a response to such shortcomings, this article presents a simulation with a 3-dimensional Norton's model, which overcomes the difficulties because it is characteristic of ceramics at high temperatures. The results of our simulated experiments show advantages with respect to the identification of the mechanisms that contribute to the final shape of the body. Our work is able to divide the history of temperatures in stages where the evolution of the thermal, elastic and creep deformations is simplified and meaningful. That is achieved because our work found that curvature is the most descriptive parameter of the simulation, the most important contribution of this article. Future work is to be realized in the creation of a model that takes into account that the shrinkage is dependent on the history of temperatures. The main shortcoming of the paper is the lack of physical experiments to corroborate the simulations.

Glossary

$\boldsymbol{H(S,p)}$:	Mean curvature of a surface *S* at a point *p*.
$\boldsymbol{H_{upp}}$:	Set of discrete mean curvatures at the nodes of the upper face of the ceramic tile.
$\boldsymbol{H_{low}}$:	Set of discrete mean curvatures at the nodes of the lower face of the ceramic tile.
$\boldsymbol{\varepsilon_{th}}$:	Set of thermal strains in one direction. Von Misses thermal strains are not defined.
$\boldsymbol{V\varepsilon_{el}}$:	Set of Von Mises elastic strains.
$\boldsymbol{V\varepsilon_{cr}}$:	Set of Von Mises creep strains.
$\boldsymbol{V\sigma}$:	Set of Von Mises stresses.
$\boldsymbol{\bar{M}}$:	Average of set $\boldsymbol{M}$. The set can be: $\boldsymbol{H_{low}}, \boldsymbol{H_{upp}}, \boldsymbol{\varepsilon_{th}}, \boldsymbol{V\varepsilon_{cr}}, \boldsymbol{V\varepsilon_{el}}$, or $\boldsymbol{V\sigma}$.
$\boldsymbol{std.dev.M}$:	Standard deviation of set $\boldsymbol{M}$.
$\boldsymbol{max(M)}$:	Maximum absolute value of set $\boldsymbol{M}$.
$\boldsymbol{\sigma_1, \sigma_2, \sigma_3}$:	Set of first principal, second principal and third principal stresses respectively.

1 Introduction

Several assumptions have to be made to model at some extent the sintering of pure ceramic materials. Some of these assumptions are: (i) no chemical reactions occur, (ii) the particles that compose the material are of the same compound and (iii) the sintering mechanisms are well defined. Because of the complexity of the materials often used to make floor and wall covering ceramic tiles, these basic assumptions do not hold. However, there is a need for computational models that can predict at least some final properties.

Computational models of the firing can have uses in the prediction of the dimensional parameters of the tile. The acceptable parameters, including curvature, are described in the standard ISO10545-2 ([1]). Predicting the curvature of the tile in the oven and after it is cooled is important for the ceramic industry, as an appreciable final curvature can cause the product to be rejected. In addition, an appreciable and non-uniform curvature during the firing can cause the decoration to be damaged or have other effects in the final properties of the tile. In our approach the mean curvature of the surface is defined at every point of the surface. The definition of mean curvature and its discretized form can be found in [2].

This article is organized as follows: Section 2 discusses the current state of art in computer simulation of ceramic tile firing. Section 3 describes the methodology used in this article, as a result of the conclusions of our literature review. Section 4 presents the results of the proposed methodology. Section 5 concludes the article.

2 Literature Review

The "fit-to-reality" approach when modeling the sintering of a ceramic solid uses full constitutive equations. Full constitutive equations include parameters obtained from the microscopic structure of the powder to calculate the shape of the body. Full constitutive equations need parameters that are complex to obtain and define. Simulations and equations do change with the stages of the sintering, so they should then be defined and considered on a specific time and context. This approach is used in [3-5]. Even for the purest ceramics, certain stages of the sintering require phenomenological parameters, that is, parameters from experimental models rather than from microstructure models. Mixed models, like the ones used in [6,7], use phenomenological constitutive equations in stages where the sintering is more complicated and full constitutive equations in stages where the microstructural parameters can be found.

Trying to reduce the number of parameters and the difficulty to obtain them, some simulations restrict their objectives. For example, they only use geometric parameters like linear shrinkage to obtain the final shape of the solid. Ref [8] presents a simulation that uses the principle of the Master Sintering Curve, ([9]), which states that the geometric parameters used in constitutive equations are functions only of density for a given powder and green-body process. The parameters used are fewer, but they have to be obtained for every powder process. This makes the experiments difficult to replicate. As usual, there is a definite shortage of reports on traditional ceramics.

In continuum mechanics, constitutive equations that do not rely in the microstructure of the material are used. Macroscopic constitutive equations that do not rely in the

microstructure are able to explain the changes of the shape using simple parameters like elastic, thermal and creep deformations; or mechanical stresses. Calculating mechanical stresses when the body is at low temperatures allows finding the possibility of brittle fracture. In traditional ceramics, the complexity of the materials and processes involved is high. This is the reason why only a macroscopic approach that does not take into account the microstructure of the material can be used. Few simulations of the firing of ceramic tiles have been made. In [10, 11] a linear approach is used to simulate the deformation of a ceramic tile. However, the behavior that stoneware, (the most common material used for floor covering ceramic tiles), shows at high temperatures is nonlinear. In [12] a nonlinear constitutive equation is used. However, the model is not characteristic of ceramics at high temperatures and it is used because it fits the data. In this reference, the authors argue that Norton's model was not used because for different forces applied to a specimen, different parameters that fit the model are obtained. The subject has been widely studied and it is known to be a characteristic of ceramics ([13, 14]). The model in [12] only considers displacements in 2 directions, which does not comply with the physical problem. In that reference, strains are averaged through the thickness of the specimen, which over-simplifies the problem.

2.1 Conclusions of the Literature Review

After reviewing the literature, the authors have found the following conclusions:

1. Full constitutive equations can only be used with engineering ceramics. Even in that case, the models are restricted.
2. The models that use geometrical parameters have only been tested with engineering ceramics and their parameters have to be obtained for every powder process.
3. Currently, models that use macroscopic constitutive equations are the only ones that can be used with traditional ceramics.
4. Previous simulations do not use a model characteristic of ceramics at high temperatures.
5. Previous simulations cannot easily evaluate the contribution of each deformation.
6. The central curvature is used to evaluate the shape of the tile. The central curvature cannot evaluate other defects like non-uniformity.

Our article will address the shortcomings in the following manner:

1. A constitutive equation from macroscopic parameters is used because, as shown in conclusions 1, 2 and 3, other approaches cannot be used with traditional ceramics.

2. We use Norton's model, which is characteristic of ceramics at high temperatures, to address conclusion 4. Norton's model is nonlinear but simply described and can be used to find elastic and creep deformations and also stresses, which addresses conclusion 5.

3. We evaluate the curvature at every point of the surface, which addresses conclusion 6.

3 Methodology

Our simulation is divided into two physical problems: (i) a thermal simulation, which calculates the distribution of temperatures in the body, and (ii) a structural simulation, which uses the temperatures to calculate the thermal deformations and the resulting stresses and mechanical strains that the thermal deformations produce. The deformation

of the ceramic tile appears because of the difference of temperatures between the lower and upper faces, which causes the body to have different expansions across the depth of the thickness.

The evolution of the different mechanical, thermal and geometric parameters of a tile with defined thickness is first evaluated. This thickness is representative and allows the observation of the evolution of the parameters of the tile independent of the thickness. After that, tiles with different thicknesses are also evaluated so the evolution of the parameters can be parameterized. The geometric parameters of the tile are shown in table 1.

Table 1: Geometric parameters of the tile.

Parameter	Value
Sides of the Tile:	33cm x 33cm.
Defined Thickness:	20mm.
Variable Thickness:	14mm, 18mm, 20mm and 24mm.

For the thermal simulation, constant different temperatures were applied at the upper and lower faces of the tile. The parameters are shown in table 2.

Table 2: Thermal parameters of the tile.

Parameter	Value
Density of the Tile (ρ):	2150 Kg/m^3
Thermal Conductivity (k):	0.57 $W/(m\,K)$
Heat Capacity (c):	1250 $J/(Kg\,K)$

The program of temperatures was characteristic of ceramic tiles firing. It can be seen in Figure 1.

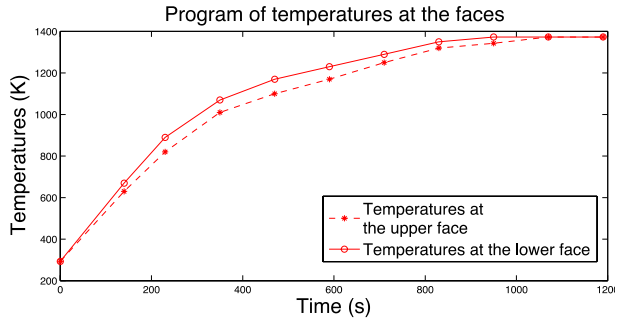

Figure 1: Temperatures in each of the surfaces of the tile as a function of time in the oven.

For the structural problem the tile is minimally constrained so equations can be formulated and solved, without restricting deformations in any direction. A linear coefficient of thermal expansion, (α), is used. The data from Ref. [12] was digitized, ([15]), and is shown in Fig. 2. Norton's model is appears in equation (1).

$$\frac{d\varepsilon(t)}{dt} = \frac{d\sigma(t)}{dt}\frac{1}{\eta} + A\,\sigma(t)^n \tag{1}$$

In equation (1), $\varepsilon(t)$ is the strain as a function of time, $\sigma(t)$ is the tensile stress, η is Young's modulus. A and n are temperature-dependent constants which define the creep behavior of Norton's model.

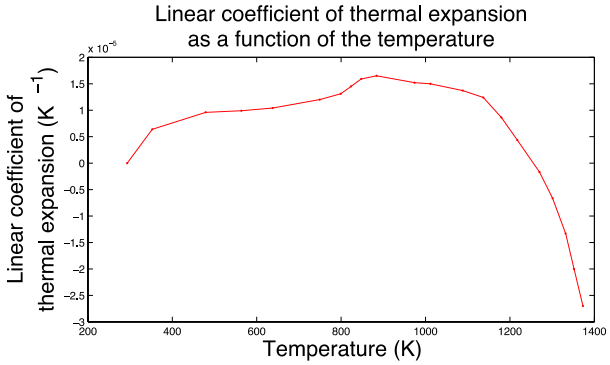

Figure 2: Linear coefficient of thermal expansion as a function of the time.

In this paper, parameters for Norton's model have been determined which fit the data from [12]. The stress-relaxation data was divided in two parts: (i) a fast application of the load in which the deformation is assumed as elastic and (ii) a measure of the stress required to maintain the strain obtained after (i). The graphs were digitized and the parameters η, A and n were obtained. Non-linear least squares regression, ([16, 17]), was used to fit the parameters, which appear in Table 3.

Table 3: Structural constants of the constitutive model for the study

$T(K)$	$\eta\ (GPa)$	$A\ (s^{-1})$	n
293.15	3.06	0	–
773.15	3.75	2.289×10^{-26}	5
973.15	4.48	4.010×10^{-28}	5
1073.15	4.63	1.164×10^{-27}	5
1173.15	6.07	1.778×10^{-21}	4.27
1173.15	6.63	5.046×10^{-8}	2.42
1273.15	6.49	1.418×10^{-6}	2.30
1323.15	3.14	7.358×10^{-7}	2.44

Our simulation used ANSYS® for the FEA (Ref. [18]). We selected the elements SOLID90 for the thermal problem and SOLID186 for the structural problem. Our simulations included large deformations. The total time spent by each simulation was around 30 days using two Core 2 Duo Processors at 2.33 GHz and 1.7 GB of RAM.

The curvatures as a function of the time have been evaluated using the algorithm from Ref. [2]. The average was calculated as $\sum H\ /\ n$, where n is the number of nodes. At the borders H has been interpolated by using the values at the neighbor nodes interior to the face.

4 Results

4.1 Evolution of the tile with defined thickness

In Fig. 3 a summary of the curvatures as function of the time is shown.

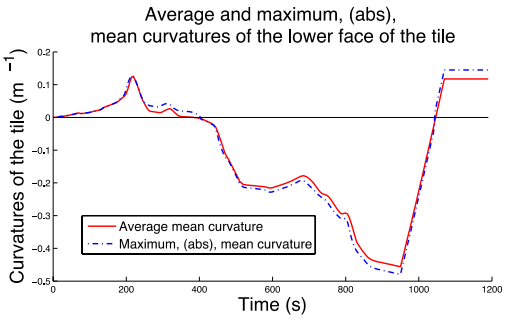

Figure 3(a): Average and maximum, (abs), mean curvatures of the lower face of the tile

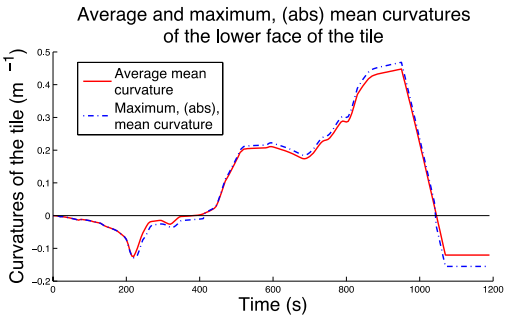

Figure 3(b): Average and maximum, (abs), mean curvatures of the upper face of the tile.

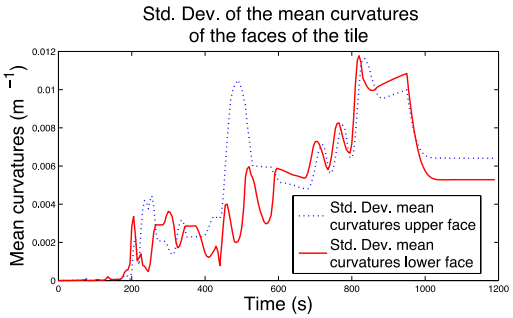

Figure 3(c): Standard deviation of the mean curvatures of the faces of the tile.

Figure 3: Figs. 3(a), 3(b) and 3(c) show $\overline{\boldsymbol{H_{low}}}$ and $\boldsymbol{max(H_{low})}$; $\overline{\boldsymbol{H_{upp}}}$; and $\boldsymbol{max(H_{upp})}$; and $\boldsymbol{std.dev.H_{low}}$ and $\boldsymbol{std.dev.H_{upp}}$, respectively, as functions of the time.

The structural problem has been created with the next 4 variables: (i) the thermal strains, (ii) the elastic strains, (iii) the creep strains and (iv) the stresses. Von Mises elastic and creep strains summarize mechanical strains while the Von Mises stresses summarize stresses. The creep formulations in ANSYS® depend on the Von Mises stresses. Since the thermal strains are equal in all directions, the Von Misses formulation cannot be applied. As an alternative, the value of the thermal strains in one direction was used to summarize them. Fig. 4 shows average, maximum and minimum stresses and strains for the tile with thickness 20mm during the time in the oven.

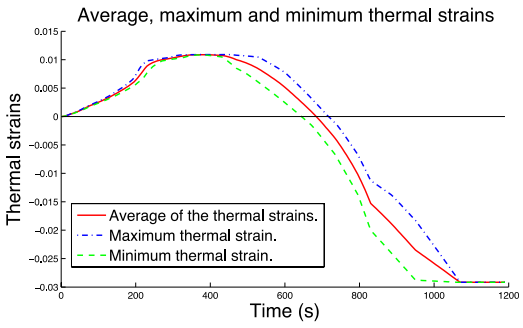

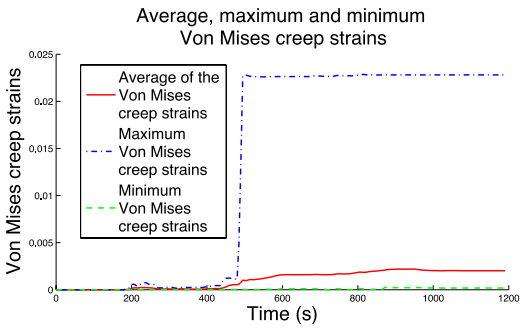

Figure 4(a): Average, maximum and minimum ε_{th} .

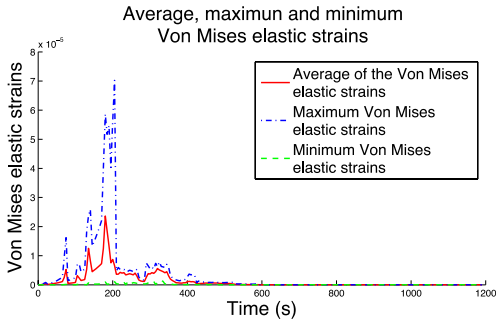

Figure 4(b): Average, maximum and minimum $V\varepsilon_{cr}$.

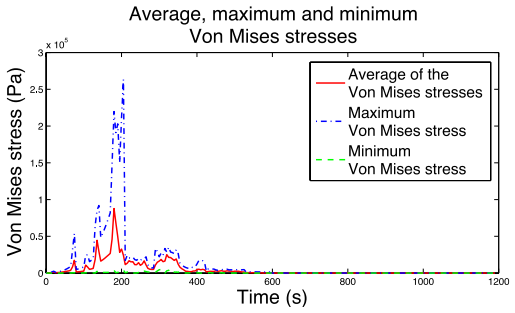

Figure 4(c): Average, maximum and minimum $V\varepsilon_{el}$.

Figure 4(d): Average, maximum and minimum $V\sigma$.

Figure 4: The evolution of strains and stresses is shown. Fig. 4(a) shows, $\boldsymbol{\varepsilon_{th}}$, Fig. 4(b) shows $\boldsymbol{V\varepsilon_{cr}}$, Fig 4(c) shows $\boldsymbol{V\varepsilon_{el}}$ and Fig. 4(d) shows $\boldsymbol{V\sigma}$.

According to the curvature, the firing of the tile can be divided in three stages:

First stage: As the ceramic body starts to expand, the lower face becomes convex and the upper one turns concave. The stage continues until the absolute values of $\overline{\boldsymbol{H_{low}}}$ and $\overline{\boldsymbol{H_{upp}}}$ reach a maximum. The maximum temperature at the end of the stage is near the temperature of the maximum thermal expansion coefficient, (T=884K, Fig. 2). This stage corresponds to the time interval [0s, 218s]. In this stage the elasticity is significantly bigger than in the rest of the measurements since the highest peaks of stresses appear and the possibility of failure because of brittle fracture is higher. The maximum stress, (0.263 MPa), is reached in the program of temperatures at t=205s. As a comparison, the mechanical strength of a ceramic tile after drying has been determined as 2.20MPa in Ref [19].

Second stage: It corresponds to the time interval [218s, 950s]. The second stage is the most important for the final properties of the tile. $\overline{\boldsymbol{V\varepsilon_{cr}}}$ becomes much higher than $\overline{\boldsymbol{V\varepsilon_{el}}}$ and the creep strains, $(\boldsymbol{V\varepsilon_{cr}})$ accumulate to contribute to the final shape of the body. In this stage, $\overline{\boldsymbol{H_{low}}}$ and $\overline{\boldsymbol{H_{upp}}}$ change sign and reach a maximum absolute value.

The second stage starts when $\overline{\boldsymbol{H_{low}}}$ begins to decrease and $\overline{\boldsymbol{H_{upp}}}$ begins to increase. $\overline{\boldsymbol{H_{low}}}$ and $\overline{\boldsymbol{H_{upp}}}$ become almost 0 at the same time, at t=383s. $\overline{\boldsymbol{H_{low}}}$ keeps decreasing until it reaches a minimum, which coincides with the time at which the lower face reaches the maximum temperature of the program, (t=950s). Fig. 5 shows the distribution of the curvatures at 950s. The amounts $\boldsymbol{std.dev.H_{low}}$ and $\boldsymbol{std.dev.H_{upp}}$ are high at t=950s . It can be seen that there are many local maxima and minima near the borders. The non-uniformity is a consequence of the high differences among the values of $\boldsymbol{V\varepsilon_{cr}}$ between the center and borders.

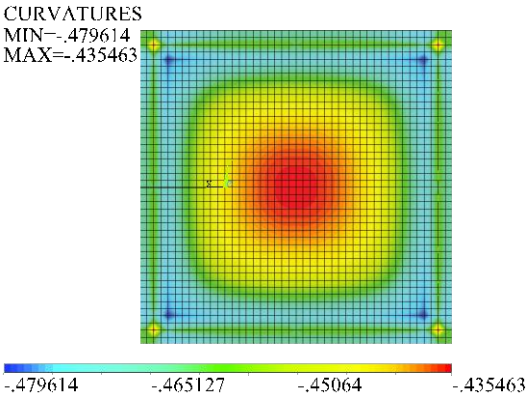

Figure 5(a): The distribution of H_{low} at 950s.

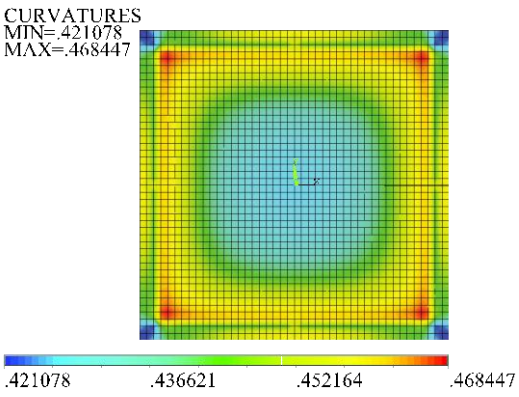

Figure 5(b): The distribution of H_{upp} at 950s.

Figure 5: The distribution of $\boldsymbol{H_{low}}$ and $\boldsymbol{H_{upp}}$ at 950*s*.

In the second stage the stresses are relaxed quickly and the deformations become more measurable. At the beginning of the stage, (t=218s), the $\overline{V\varepsilon_{cr}}$ in the upper face is higher than in the lower face. This is reversed as the curvature changes of sign. At the end of the stage (t=950s) the $\overline{V\varepsilon_{cr}}$ are higher in the lower face.

The stresses that produce the creep strains are reactions to the difference of expansions caused by the geometrical gradient of temperatures. Fig. 6 displays the first principal stresses, ($\boldsymbol{\sigma_1}$), and the third principal stresses, ($\boldsymbol{\sigma_3}$). The lower face shows positive values for $\boldsymbol{\sigma_1}$. The upper face shows negative values for $\boldsymbol{\sigma_3}$. The lower face is mostly in tension and the upper face mostly in compression, so creep strains should expand the lower face more than the upper. Even when at the end of the second stage the lower face is concave and the upper one is convex, which would seem counterintuitive. All the second stage has the characteristic that $\boldsymbol{\sigma_1}$ is higher in the lower face than in the upper one. The distribution of stresses during the second stage, and the consequent creep strain determine the geometry at the end of the third stage. Fig. 6(b) illustrates that $\overline{V\varepsilon_{cr}}$ decreases and becomes stable in the third stage.

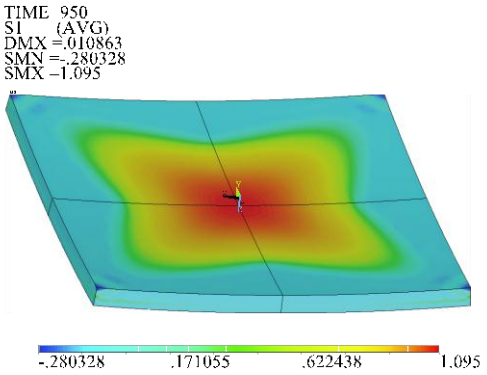

Figure 6(a): Distribution of the first principal stresses (in Pa) at 950s at the lower face of the tile.

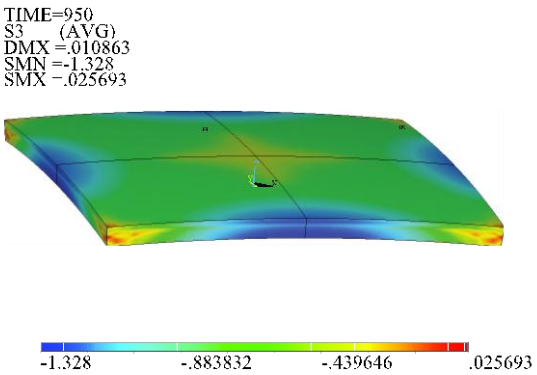

Figure 6(b): Distribution of the third principal stresses (in Pa) at 950s, at the upper face of the tile.

Figure 6: Distribution of the first and third principal stresses at 950*s*.

Third stage: It occurs as the differences in the temperature of the body are eliminated. The lower face reaches the maximum temperature at the beginning of the third stage, at 950*s*. $\overline{H_{low}}$ increases and $\overline{H_{upp}}$ decreases until the temperature of the upper face also reaches the maximum (at 1070*s*). The change of $\overline{H_{low}}$ and $\overline{H_{upp}}$ between 950*s* and 1070*s* is linear. When the temperature becomes uniform and the residual stresses start to relax, $\overline{H_{low}}$ is positive and and $\overline{H_{upp}}$ is negative. At the end of the program, $\overline{V\sigma}$ and $\overline{V\varepsilon_{el}}$ are low. $\overline{H_{low}}$ at the end of the third stage is higher than $\overline{H_{low}}$ at the end of the first stage (which is a local maximum and the maximum of the first stage).

4.2 Comparison of the Evolution of Ceramic Tiles with Variable Thickness During the Firing

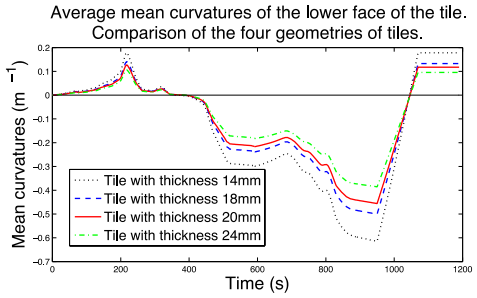

Figure 7(a): Average of H_{low} of the four geometries of tiles as a function of the oven time.

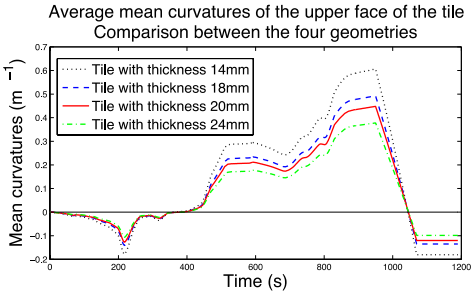

Figure 7(b): Average of H_{upp} of the four geometries of tiles as a function of oven time.

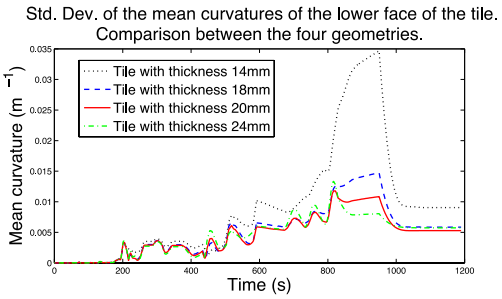

Figure 7(c): Std. dev. of H_{low} of the four geometries of tiles as a function of the oven time.

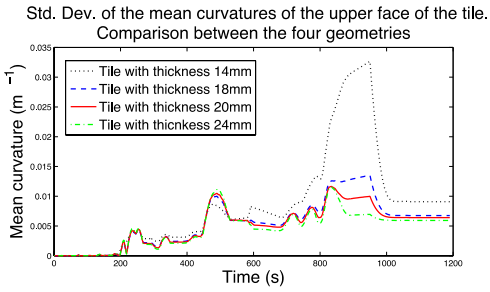

Figure 7(d): Std. dev. of H_{upp} of the four geometries of tiles as a function of the oven time.

Figure 7: Figs. 7(a) and 7(b) show $\overline{H_{low}}$ and $\overline{H_{upp}}$ for the four geometries of ceramic tiles. Figs. 7(c) and 7(d) show $std.dev.H_{low}$ and $std.dev.H_{upp}$ for both faces for the four geometries of ceramic tiles.

The stages that appeared in the 20mm ceramic tile also appeared in the rest of the geometries. This means that the stages of the mean curvature are only dependent on the program of temperatures and the properties of the tile. They do not depend on the thickness.

Fig. 7 displays the evolution of Mean Curvature and its Standard Deviation along the time axis, for 4 thickness levels. Figs 7(a) and 7(b) show the evolution of Mean Curvatures in the lower and upper face, respectively. Figs 7(c) and 7(d) illustrate the evolution of the Standard Deviation of the Mean Curvature, for the analog cases.

Fig. 8(a) shows the average creep strains for the 4 geometries. Elastic strains appear in Fig. 8(b)) and stresses appear in Fig. 8(c).

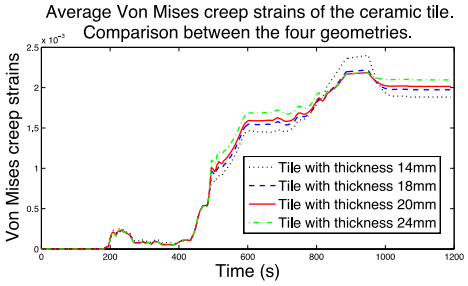

Figure 8(a): Average of $V\varepsilon_{cr}$ of the four geometries of tiles as a function of oven time.

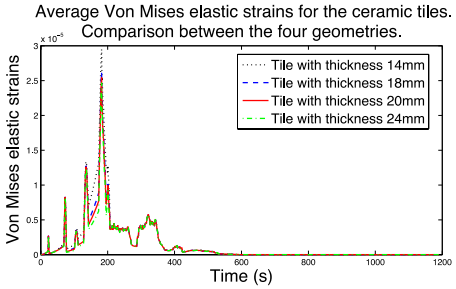

Figure 8(b): Average of $V\varepsilon_{el}$ of the four geometries of tiles as a function of oven time.

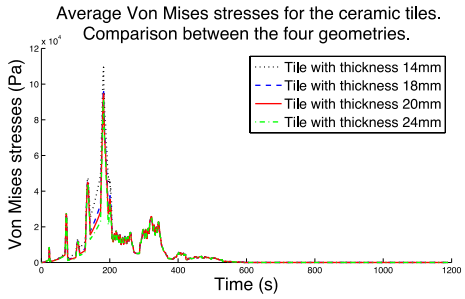

Figure 8(c): Average of $V\sigma$ of the four geometries.

Figure 8: $\overline{V\varepsilon_{el}}$, $\overline{V\varepsilon_{cr}}$ and $\overline{V\sigma}$ of the four geometries of tiles as a function of the time.

The absolute $\overline{H_{low}}$ and $\overline{H_{upp}}$ increase as the tile thickness decreases. The shapes of the curves were similar, with steeper slopes in the thinner models. $Std.devs.H_{low}$ and $std.devs.H_{upp}$ are higher for the thinnest tiles. However, the shapes of the curves are very different, and the curves show a more sensitive behavior to the reduction of thickness than to $\bar{H}$.

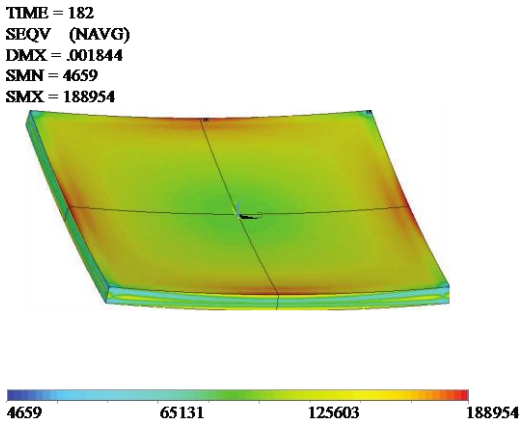

Figure 9: Tile that shows the maximum $V\sigma$ for the ceramic tile with defined thickness.

The maximum $V\sigma$ are the following: (i) thickness=14mm, stress=0.474MPa, t= 205s, (ii) thickness=18mm, stress=0.314MPa, t=205s, (iii) thickness=20mm, stress=0.263MPa, t=205s and (iv) thickness=24mm, stress=0.197MPa, t=201s. Fig. 9 shows $V\sigma$ for the tile with thickness=20mm and t=182s. At that time, the $\overline{V\sigma}$ for the tile was the maximum. The figure shows that the maximum stresses appear near the middle of the borders of the tile.

5 Discussion and Conclusions

A flat tile is a goal of the firing itself. The evaluation of the curvature at every point of the tile allows the manufacturer to control more appropriately the temperature in stages where de differences of the curvatures are more notorious. This paper shows that the curvature also helps to divide the firing into stages of the history of temperatures. These stages help to isolate the different effects of the viscoelastic constitutive equation and the thermal expansion of the body. The curvature changes in a more predictable way than the rest of the physical parameters evaluated. The main conclusion of the simulated tests is that the curvature is the most determinant parameter of the history of temperatures and the most important parameter to control when designing a program of temperatures. Other conclusions of the paper are:

1) The magnitudes of $\overline{H_{low}}$ and $\overline{H_{upp}}$ decrease as the thickness increases, but the local maximums appear at the same time. The shape of the curve of $std.dev.H_{low}$ and $std.dev.H_{upp}$ is not the same for all the thicknesses, but the values are higher with thinner tiles. $Std.dev.H_{low}$ and $std.dev.H_{upp}$ are reflected in the homogeneity of the surfaces. The distribution of curvatures indicates that the measurements at different points of the tile are necessary to control the shape of the tile.

2) The tile at low temperatures has a brittle behavior. To evaluate the possibility of brittle fracture, more constants than just mechanical strength are needed and they have to be measured at high temperatures. However, the maximum $V\sigma$ reached by the thinnest tile is much lower than the maximum mechanical strength measured on the dry tile ([19]). On the other hand, deformations caused by creep are significant and the defects caused by creep are important and cause concern in the manufacturers.

3) When the temperature becomes uniform, (and no stresses exist), the curvature of the tile is opposite to the sign that the thermal expansion forces on the tile that prevail most of the oven time.

5.1 Future Work

Future work is needed in the creation of a model that takes into account that the shrinkage is dependent on the history of temperatures. In this manner, we are able to simulate the time interval in the oven when the temperature is sharply decreased until the tile is cold and the curvature stabilizes. Intensive experimental work is also needed to corroborate the simulations .

References

[1] ISO. 10545-2:1995: Ceramic tiles – part 2: Determination of dimensions and surface quality. International standard confirmed, International Organization for Standardization, Geneva, Switzerland, 31-12 2005.

[2] M. Botsch and M. Pauly. Course 23: Geometric modeling based on polygonal meshes. In *ACM SIGGRAPH 2007 courses*, 2007.

[3] E.A. Olevsky and V. Tikare. Combined macro-meso scale modeling of sintering. part i: Continuum approach. *Recent Developments in Computer Modeling of Powder Metallurgy Processes*, page 85, 2001.

[4] V. Tikare, E.A. Olevsky, and M.V. Braginsky. Combined macro-meso scale modeling of sintering. Part II, Mesoscale simulations. *Recent Developments in Computer Modeling of Powder Metallurgy Processes*, page 94, 2001.

[5] K. Shinagawa. Finite element simulation of sintering process: Microscopic modelling of powder compacts and constitutive equation for sintering. *JSME international journal. Series A, mechanics and material engineering*, 39(4):565–572, 1996.

[6] H. Riedel Torsten Kraft. Numerical simulation of solid state sintering; model and application. *Journal of the European Ceramic Society*, 24:345–361, 2004.

[7] H. Riedel and B. Blug. A comprehensive model for solid state sintering and its application to silicon carbide. *Solid Mechanics and Its Applications*, 84:49–70, 2001.

[8] J. A. Yeomans, M. Barriere, P. Blanchart, S. Kiani, Jingzhe Pan. Finite element analysis of sintering deformation using densification data instead of a constitutive law. *Journal of the European Ceramic Society*, 27:2377–2383, 2007.

[9] Hunghai Su and D. Lynn Johnsonn. Master sintering curve: A practical approach to sintering. *Journal of the American Ceramic Society*, 79(12):3211–17, 1996.

[10] H. Camacho, M. E. Fuentes, L. Fuentes, A. Garcia, and Perez A. Stress distribution evolution in a ceramic body during firing. part 1. problem statement. volume 42, pages 283–288. *Bol. Soc. Esp. Ceram.*, 2003.

[11] H. Camacho, M. E. Fuentes, L. Fuentes, A. Garcia, and Perez A. Stress distribution evolution in a ceramic body during firing. part 2. profile calculation. volume 42, pages 353–359. *Bol. Soc. Esp. Ceram.*, 2003.

[12] V. Cantavella Soler et al. Simulación de la deformación de baldosas cerámicas durante la cocción. PhD thesis, 1998.

[13] W.R. Cannon and T.G. Langdon. Review: creep of ceramics, part 1: Mechanical characteristics. *J. Mater. Sci*, 18(1):1–50, 1983.

[14] W.R. Cannon and T.G. Langdon. Review: Creep of ceramics, part 2: An examination of flow mechanisms. *J. Mater. Sci.*, 23:1–20, 1988.

[15] M. Mitchell. *Engauge Digitizer*, 2009.

[16] R Development Core Team. R: A Language and Environment for Statistical Computing. *R Foundation for Statistical Computing*, Vienna, Austria, 2009. ISBN 3-900051-07-0.

[17] G. Grothendieck. nls2: Non-linear regression with brute force. R package version 0.1-2. 2007.

[18] J. Swanson. Ansys 11.0, Ansys, 2008.

[19] J. L. Amoros, E. Sanchez, V. Cantavella, and JC Jarque. Evolution of the mechanical strength of industrially dried ceramic tiles during storage. *Journal of the European Ceramic Society*, 23(11):1839–1845, 2003.